ARTICLE

Doxorubicin-Tethered Responsive Gold Nanoparticles Facilitate Intracellular Drug Delivery for Overcoming Multidrug Resistance in Cancer Cells

Feng Wang,[‡,⊥] Yu-Cai Wang,[§,⊥] Shuang Dou,[†] Meng-Hua Xiong,[§] Tian-Meng Sun,[‡] and Jun Wang[†,*]

[†]CAS Key Laboratory of Brain Function and Disease, and School of Life Sciences, University of Science and Technology of China, Hefei, Anhui 230027, P. R. China, [‡]Hefei National Laboratory for Physical Sciences at the Microscale, and School of Life Sciences, University of Science and Technology of China, Hefei, Anhui 230027, P. R. China, and [§]Department of Polymer Science and Engineering, University of Science and Technology of China, Hefei, Anhui 230026, P. R. China. [⊥]These authors contributed equally to this work.

ABSTRACT Multidrug resistance (MDR) is a major impediment to the success of cancer chemotherapy. Through the development of a drug delivery system that tethers doxorubicin onto the surface of gold nanoparticles with a poly(ethylene glycol) spacer *via* an acid-labile linkage (DOX-Hyd@AuNPs), we have demonstrated that multidrug resistance in cancer cells can be significantly overcome by a combination of highly efficient cellular entry and a responsive intracellular release of doxorubicin from the gold nanoparticles in acidic organelles. DOX-Hyd@AuNPs achieved enhanced drug accumulation and retention in multidrug resistant MCF-7/ADR cancer cells when it was compared with free doxorubicin. It released doxorubicin in response to the pH of acidic organelles following endocytosis, opposite to the noneffective drug release from doxorubicin-tethered gold nanoparticles *via* the carbamate linkage (DOX-Cbm@AuNPs), which was shown by the recovered fluorescence of doxorubicin from quenching due to the nanosurface energy transfer between the doxorubicinyl groups and the gold nanoparticles. DOX-Hyd@AuNPs therefore significantly enhanced the cytotoxicity of doxorubicin and induced elevated apoptosis of MCF-7/ADR cancer cells. With a combined therapeutic potential and ability to probe drug release, DOX-Hyd@AuNPs represent a model with dual roles in overcoming MDR in cancer cells and probing the intracellular release of drug from its delivery system.

KEYWORDS: gold nanoparticles · multidrug resistance · drug delivery · doxorubicin · nanosurface energy transfer · intracellular drug release

The development of multidrug resistance (MDR) has been a major impediment to the success of cancer chemotherapy and interest is growing in the development of drug delivery systems using nanotechnology to reverse MDR in cancer.[1−3] As one of the most important mechanisms involved in many MDR cells, P-glycoprotein (P-gp), a membrane-bound active drug efflux pump, is an important transporter and is capable of effluxing a broad range of structurally and functionally distinct anticancer agents, which is often overexpressed in the plasma membrane of many MDR cells.[4,5] Therefore, inhibition, or bypass, of P-gp-mediated drug efflux or P-gp expression has become an important strategy in overcoming MDR. For example, it has been validated that Pluronic polymers sensitize MDR cells to a few cytotoxic drugs by inhibiting the P-gp drug efflux system and affecting several other drug resistance mechanisms.[6−8] In other examples, by applying multifunctional nanoparticles, for example, anionic liposome−polycation−DNA complexes (LPD-II) and mesoporous silica nanoparticles, siRNAs targeting the gene encoding P-gp have been delivered into MDR cells to downregulate P-gp expression, thereby helping to restore intracellular drug levels to the concentrations required for induction of cytotoxicity.[9] Thus, simultaneously codelivering cytotoxic drugs by these same nanoparticles exerts enhanced efficiency in inhibiting growth of MDR cells.[9,10] Other nanoparticle-based approaches, such as by rendering the drug inaccessible to the P-gp efflux pump in MDR cells, have also been reported to overcome MDR in cancer.[11−16] As a typical example, Bae's group reported that doxorubicin-loaded polymeric micellar nanoparticles can overcome cancer MDR by targeting both the folate receptor and early endosomal pH.[17,18]

Nanoparticles can enter cells by an endocytosis pathway, which may be mediated by clathrin, caveolae, macropinocytosis, or phagocytosis.[19−21] Many studies have indicated that exocytosis of nanoparticles may be independent from the P-gp pathway,[22−24] in other words, nanoparticles may not be the substrate of P-gp. Thus, it can be expected that an ideal nanoparticular delivery system that can significantly overcome MDR would be

* Address correspondence to: jwang699@ustc.edu.cn.

Received for review January 3, 2011 and accepted April 4, 2011.

Published online April 04, 2011
10.1021/nn200007z

© 2011 American Chemical Society

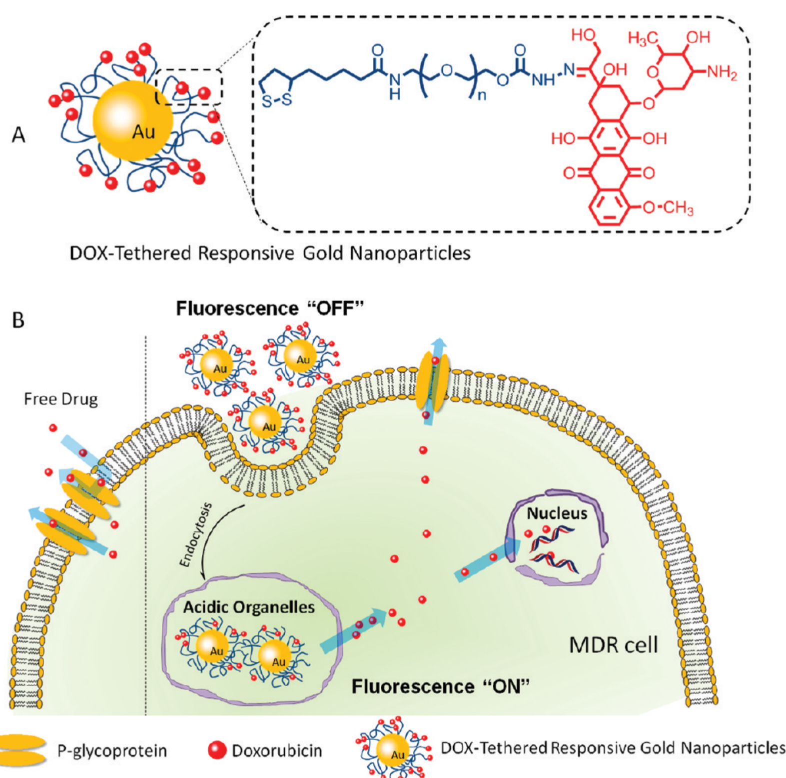

Scheme 1. (A) Schematic illustration of doxorubicin (DOX)-tethered responsive gold nanoparticles. (B) Schematic illustration of the cooperation between enhanced doxorubicin cellular entry and a responsive intracellular release of doxorubicin into the cells to overcome drug resistance. The fluorescence of doxorubicin tethered to gold nanoparticles is quenched (Fluorescence "OFF"), while recovered when it is released with response to cellular acid conditions (Fluorescence "ON").

dependent on the high efficiency of cellular entry of the nanoparticles and subsequent rapid release of the cytotoxic drug intracellularly that should be sufficiently high to induce cytotoxicity. Gold nanoparticles (AuNPs), which are known to be inert, have shown advantages and significant progress in the delivery of small molecules to large biomacromolecules, including DNA, siRNA, and proteins.[25−30] On the other hand, recent studies have indicated that AuNPs act as good quenchers of many fluorescence donors, due to the nanosurface energy transfer (NSET) effect.[31−33] This may render AuNPs as the base of a fluorescent "nanoprobe", particularly useful in the trafficking of intracellular drug release, by monitoring changes in fluorescence. In this study, we developed a drug delivery system by tethering doxorubicin onto the surface of AuNPs with a poly(ethylene glycol) spacer *via* an acid-labile linkage (Scheme 1), which can significantly overcome P-gp-mediated drug resistance by a combination of enhanced doxorubicin cellular entry and a responsive intracellular release of doxorubicin in acidic organelles. In addition, the intracellular responsive release of doxorubicin from AuNPs was monitored and visualized following the recovery of fluorescence signals quenched by AuNPs.

RESULTS AND DISCUSSION

Preparation and Characterization of DOX-Tethered AuNPs. To obtain doxorubicin-tethered AuNPs with a rapid response to the acidity of acidic organelles or compartments, we first synthesized heterofunctional α-lipoyl-ω-doxorubicinyl poly(ethylene glycol) with a hydrazone linker between the doxorubicinyl group and the poly(ethylene glycol) chain (further denoted as LA-PEG-Hyd-DOX). As shown in Figure 1, synthesis started from α-hydroxy-ω-amino-poly(ethylene glycol) (HO-PEG-NH_2, MW = 3400), which was first condensed with α-lipoic acid to give α-lipoyl-ω-hydroxy poly(ethylene glycol) (LA-PEG-OH). The hydroxyl group of LA-PEG-OH was then activated with *p*-nitrophenyl chloroformate, generating LA-PEG-NPC, which was further reacted with hydrazine monohydrate to give LA-PEG-Hyd. LA-PEG-Hyd-DOX was obtained by conjugating doxorubicin to LA-PEG-Hyd by a hydrazone linker. As a control, doxorubicin was also conjugated to LA-PEG-NPC to generate LA-PEG-Cbm-DOX, which contained a carbamate linker between the doxorubicinyl group and the poly(ethylene glycol) chain. The detailed characterizations of the intermediates, LA-PEG-Hyd-DOX and LA-PEG-Cbm-DOX by ^1H NMR analyses, are shown in the Supporting Information (Figures S1−S5). The extents of doxorubicin conjugation to PEG of both LA-PEG-Hyd-DOX and LA-PEG-Cbm-DOX were approximately 100% from the ^1H NMR analyses.

The hydrazone linker is hydrolytically cleavable, particularly at low pH values.[34] As shown in Figure 2, LA-PEG-Hyd-DOX exhibited a monodispersed peak at

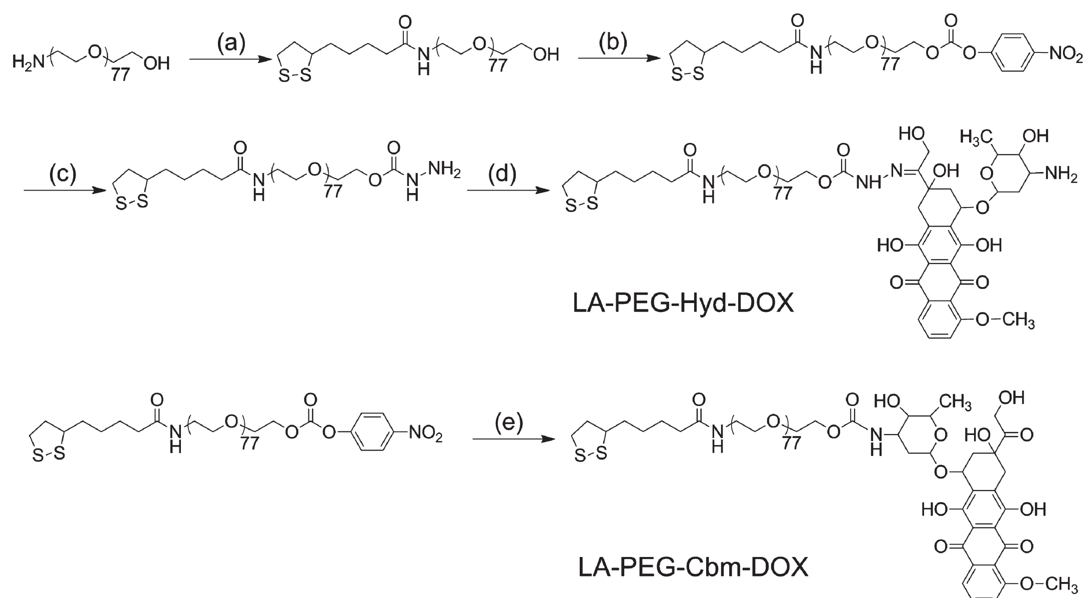

Figure 1. Syntheses of α-lipoyl-ω-doxorubicinyl poly(ethylene glycol) with a hydrazone linker (LA-PEG-Hyd-DOX) or with a carbamate linker (LA-PEG-Cbm-DOX). (a) α-lipoic acid, *N,N′*-dicyclohexyl carbodiimide, triethylamine, dichloromethane; (b) *p*-nitrophenyl chloroformate, triethylamine, dichloromethane; (c) hydrazine monohydrate, dichloromethane; (d) doxorubicin, trifluoroacetic acid, methanol; (e) doxorubicin, triethylamine, *N,N′*-dimethylformamide.

an elution time of 4.0 min (trace 2) when analyzed by high performance liquid chromatography (HPLC) with a fluorescence detector, while free doxorubicin was eluted at 1.6 min (trace 1). Incubation of LA-PEG-Hyd-DOX at pH 5.0 for 1 h led to partial degradation of the hydrazone bonds, resulting in two separate elution peaks (trace 3), corresponding to doxorubicin and LA-PEG-Hyd-DOX, respectively. However, treatment of LA-PEG-Hyd-DOX at an even lower pH of 1.0 for 1 h completely degraded the hydrazone bonds of LA-PEG-Hyd-DOX (trace 4), indicating the accelerated hydrolization of hydrazone bonds at the low pH. However, LA-PEG-Cbm-DOX, with a carbamate linker, did not significantly degrade after incubation at pH 1.0 for 1 h (trace 6).

AuNPs stabilized with citric acid were prepared according to the procedure reported in the literature.[35] The nanoparticles were roughly spherical and the average diameter was around 30 nm as determined by transmission electron microscopy (TEM) (Figure 3A, upper). LA-PEG-Cbm-DOX or LA-PEG-Hyd-DOX was anchored onto the surface of AuNPs *via* Au−disulfide interactions, generating doxorubicin-tethered DOX-Cbm@AuNPs or DOX-Hyd@AuNPs, respectively, which was purified by centrifugation to remove free LA-PEG-Cbm-DOX or LA-PEG-Hyd-DOX. No self-aggregation was observed during the conjugation of heterofunctional α-lipoyl-ω-doxorubicinyl poly(ethylene glycol) to the surface of AuNPs, and the doxorubicin-tethered AuNPs could be easily resuspended in aqueous solution. A typical proof relied on the UV−vis absorption spectrum of DOX-Hyd@AuNPs shown in Supporting Information, Figure S6, which exhibited a slight red shift (2 nm) of λ_{max} when compared to that of citric acid-stabilized AuNPs, but there was no change in other optical properties. Such a phenomenon suggested no self-aggregation of DOX-Hyd@AuNPs and it indicated the successful conjugation of LA-PEG-Hyd-DOX to the surface of AuNPs.[36,37] A similar spectrum of DOX-Cbm@AuNPs was observed (result not given). The image of DOX-Hyd@AuNPs observed by TEM exhibited a thin polymer layer, surrounding the AuNPs with an approximately 2−3 nm thickness (Figure 3A, lower). The amount of LA-PEG-Hyd-DOX conjugated to the AuNPs was 17.0 ± 2.0% by weight ratio (LA-PEG-Hyd-DOX to AuNPs), calculated from HPLC analysis results of LA-PEG-Hyd-DOX in the supernatant of the reaction mixture after centrifugation. In consideration of the face centered cubic structure of atoms in gold nanoparticles,[38] the molar mass of gold nanoparticles is about 1.64×10^8 g/mol, while the grafting number of DOX-PEG conjugate on each particle is around 8400.

It is worth noting that the fluorescence emission intensity of LA-PEG-Hyd-DOX significantly decreased after the reaction with AuNPs. When the concentration of LA-PEG-Hyd-DOX was fixed at 10 μM, the increase in AuNPs concentration from 0 to 3000 pM in the reaction solution resulted in a significant increase in doxorubicin fluorescence quenching (Figure 3B), demonstrating the presence of nanosurface energy transfer (NSET) between the doxorubicinyl groups and AuNPs. This phenomenon indeed indicated the formation of doxorubicin-tethered AuNPs since mixing free doxorubicin with AuNPs did not significantly give fluorescence quenching. Our experimental data showed a quenching efficiency of nearly 97% when the concentration of AuNPs reached 1500 pM; while nearly 100% when the concentration of AuNPs reached

3000 pM (Figure 3B). The Stern–Volmer quenching constant (K_{SV}) was calculated on the basis of eq 1 according to the reference, in which ϕ_0 and F_0 are quantum yield and emission intensity at 565 nm in the absence of the nanoparticle quencher; ϕ and F are the same parameters in the presence of the nanoparticle quencher; $[C_Q]$ is the concentration of the nanoparticle quencher.[31,39]

$$\frac{\phi_0}{\phi} = \frac{F_0}{F} = 1 + K_{SV}[C_Q] \quad (1)$$

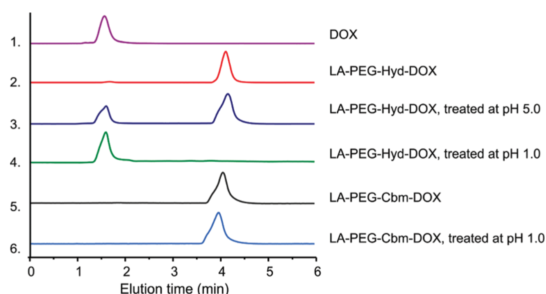

Figure 2. Analyses of the stability of LA-PEG-Hyd-DOX and LA-PEG-Cbm-DOX by reverse-phase high performance liquid chromatography. Trace (1) doxorubicin (DOX), (2) LA-PEG-Hyd-DOX, (3) LA-PEG-Hyd-DOX after incubation at pH 5.0 for 1 h, (4) LA-PEG-Hyd-DOX after incubation at pH 1.0 for 1 h, (5) LA-PEG-Cbm-DOX, (6) LA-PEG-Cbm-DOX after incubation at pH 1.0 for 1 h.

Linear dependence of F_0/F on the concentration of AuNPs was depicted in Figure 3C, which exhibited a slope of K_{SV} = 1.16 × 10^{10} M^{-1}, revealing high quenching efficiency of doxorubicin by AuNPs. Careful comparison of the emission spectra revealed the decreased ratio of intensities at 565 and 595 nm (I_{565}/I_{595}) upon addition of AuNPs (Figure 3B and Supporting Information, Figure S7A), while the I_{565}/I_{595} of free doxorubicin aqueous solution did not obviously change upon dilution with water (Supporting Information, Figure S7B). Figure 3D showed highly overlaid emission spectrum of doxorubicin with the UV–vis absorption spectrum of AuNPs. Since the fluorescence emission of doxorubicin at 565 nm is more overlaid with the absorbance spectrum of AuNPs than that at 595 nm (Figure 3D), it is reasonable to conclude that the decrease of fluorescence intensity of doxorubicin and the I_{565}/I_{595} ratio is due to the energy transfer from doxorubicin to AuNPs, which results in quenching of doxorubicin fluorescence. It has been reported that the fluorescence quenching efficiency in an NSET model is dependent on the distance between the donor and the quencher,[40] which in this case are the doxorubicinyl groups and AuNPs (Figure 3E), respectively. The energy transfer efficiency is inversely proportional to the fourth power of the distance between the donor and the

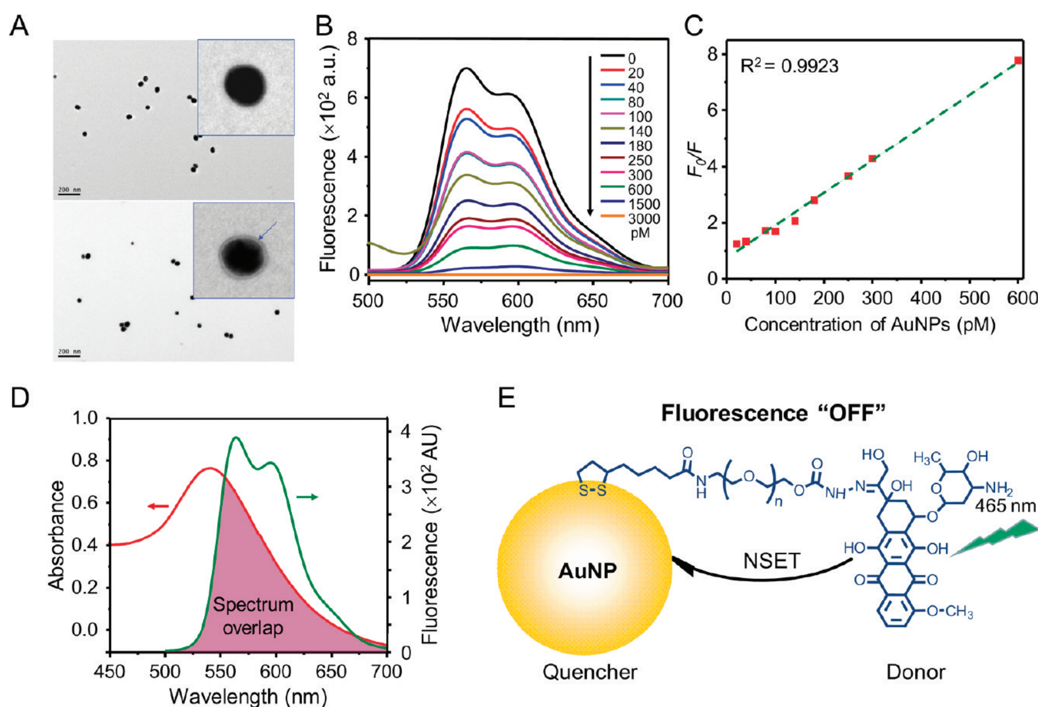

Figure 3. (A) Transmission electron microscopic image of citric acid-stabilized AuNPs (upper) and DOX-Hyd@AuNPs (lower) (scale = 200 nm). (B) Fluorescent intensity change of LA-PEG-Hyd-DOX (10 μM) after reaction with citric acid-stabilized AuNPs at different concentration from 0 to 3000 pM. Excitation wavelength = 465 nm. (C) Dependence of F_0/F on the concentration of AuNPs, F_0 is the fluorescence emission intensity of LA-PEG-Hyd-DOX in the absence of AuNPs; F is the fluorescence emission intensity in the presence of AuNPs. (D) Overlay of the UV–vis absorption spectrum of citric acid-stabilized AuNPs (red line) and the fluorescence emission spectrum of LA-PEG-Hyd-DOX (green line). (E) Schematic illustration of the nanosurface energy transfer (NSET) of doxorubicin-tethered AuNPs. The AuNPs and doxorubicinyl groups functioned as the "quencher" and the "donor", respectively.

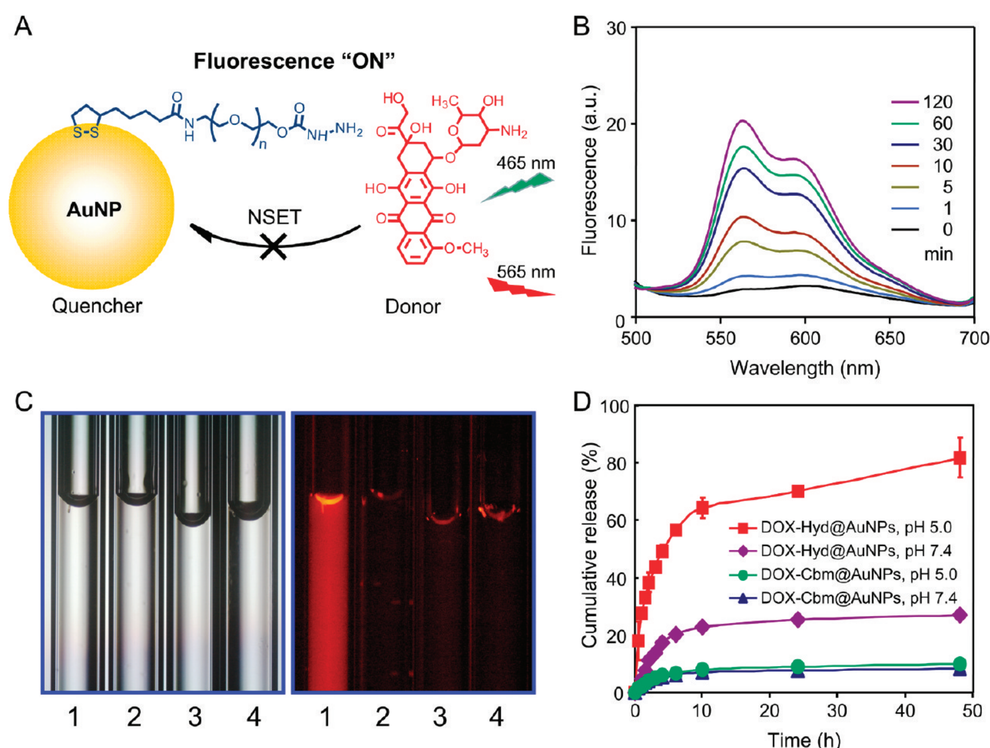

Figure 4. (A) Schematic illustration of fluorescence recovery after the degradation of hydrazone bonds in DOX-Hyd@AuNPs. (B) Fluorescence emission spectra of DOX-Hyd@AuNPs after incubation in acetate buffer (pH 5.0, 0.02 M) for different periods of time. (C) Bright field (left) and fluorescence images (right) of nanoparticles at 1 nM in capillaries after different treatments: (1) DOX-Hyd@AuNPs incubated at pH 5.0 for 1 h, (2) DOX-Hyd@AuNPs incubated at pH 7.4 for 1 h, (3) DOX-Cbm@AuNPs incubated at pH 5.0 for 1 h, (4) DOX-Cbm@AuNPs incubated at pH 7.4 for 1 h. (D) Quantitative analyses of the *in vitro* release of doxorubicin at 37 °C from doxorubicin-tethered AuNPs at pH 7.4 or in acetate buffer at pH 5.0.

quencher.[40] Therefore, it is understandable that mixing free doxorubicin with AuNPs will not lead to NSET or significant fluorescence quenching, while tethering LA-PEG-Hyd-DOX onto the surface of AuNPs will shorten the distance between the donor and the quencher and subsequently quench the fluorescence of doxorubicin.

pH-Responsive Release of Doxorubicin from Doxorubicin-Tethered AuNPs. The degradation of hydrazone bonds of DOX-Hyd@AuNPs will result in the release of doxorubicin from the nanoparticles. As discussed above, the quenched fluorescence of doxorubicin recovers once doxorubicin is released from the nanoparticles, following the degradation of hydrazone bonds due to the cessation of NSET (Figure 4A). To demonstrate this, we incubated DOX-Hyd@AuNPs in acetate buffer at pH 5.0 and measured the fluorescence emission spectrum at different time intervals. As shown in Figure 4B, incubation of DOX-Hyd@AuNPs at pH 5.0 led to rapid recovery of fluorescence. However, incubation of DOX-Hyd@AuNPs in phosphate buffered saline (PBS) at pH 7.4 did not exhibit significant fluorescence recovery after 2 h incubation (Supporting Information, Figure S8). These data demonstrate that the release of doxorubicin from DOX-Hyd@AuNPs is responsive to acidic pH. Figure 4C illustrates the fluorescence images of nanoparticles in capillaries after different treatments, where the treatment of DOX-Hyd@AuNPs at pH 5.0 resulted in high fluorescence intensity due to the release of doxorubicin from the nanoparticles and subsequent fluorescence recovery. However, DOX-Hyd@AuNPs incubated at pH 7.4 did not show bright fluorescence. Moreover, incubation of DOX-Cbm@AuNPs at pH 7.4 or pH 5.0 did not recover the fluorescence of doxorubicin.

To quantitatively determine doxorubicin release from the nanoparticles, doxorubicin-tethered AuNPs were suspended in either PBS at pH 7.4 or acetate buffer at pH 5.0 in a dialysis membrane tubing at 37 °C. The amount of released doxorubicin at predetermined time intervals was measured by HPLC. The results shown in Figure 4D reveal a release of up to around 20% of the total doxorubicin from DOX-Hyd@AuNPs after 48 h of incubation at pH 7.4. However, a much faster release of doxorubicin was observed when DOX-Hyd@AuNPs were incubated at pH 5.0, reaching 80% of cumulative release under otherwise identical conditions. These data demonstrated that the cleavage of hydrazone linkers was accelerated at lower pH values. Nevertheless, the release of doxorubicin from DOX-Cbm@AuNPs was minimal. The cumulative release of doxorubicin from DOX-Cbm@AuNPs was only about 7% in 48 h, while the release rate was independent from the pH of the medium.

Accumulation and Retention of Doxorubicin in MDR Cancer Cells. Here, a multidrug resistant cancer cell line,

MCF-7/ADR, which was obtained by continuous culture of parental MCF-7 cells in doxorubicin and maintained with doxorubicin at a dose of 1 μg mL^{-1}, was selected to test the efficiency of DOX-Hyd@AuNPs in overcoming multidrug resistance.[41−43]

The drug resistance of MCF-7/ADR was demonstrated by the overexpression of the P-gp-encoding MDR1 gene and the P-gp protein, when compared with the parental MCF-7 cells (Supporting Information, Figure S9A and S9B). P-gp is a member of the MDR/TAP subfamily, which is involved in multidrug resistance and is an ATP-dependent drug efflux pump for xenobiotic compounds with broad substrate specificity.[44] It is also responsible for decreased drug accumulation in MDR cells and often mediates the development of resistance to anticancer drugs.[4,5] Because of the overexpression of P-gp, MCF-7/ADR cells showed a high tolerance when treated with free doxorubicin, as compared to that of its counterpart wild-type MCF-7 cells, in the MTT assays (Supporting Information, Figure S9C). The simultaneous resistance of MCF-7/ADR to different drugs—a trait known as multidrug resistance or cross resistance was proven by treating the cells with epirubicin, another anthracycline drug commonly used in chemotherapy (Supporting Information, Figure S9D).

We next demonstrated whether doxorubicin-tethered AuNPs could help drug accumulation and retention in MCF-7/ADR cells. Free doxorubicin or doxorubicin-tethered AuNPs in culture medium was incubated with either MCF-7/ADR or MCF-7 cells at 5 μg mL^{-1} of doxorubicin or an equivalent dose. At different time intervals from 1 to 24 h, the extracellular medium was discarded and intracellular doxorubicin accumulation was quantitatively determined by analyses of doxorubicin concentration in the cell lysates, which were normalized to total cellular protein content of the cells. It should be mentioned that the fluorescence intensity of doxorubicin conjugated to PEG was similar to that of doxorubicin at the same pH and molar concentration. Figure 5A and 5B illustrate the intracellular accumulation of doxorubicin (or equivalent) in MCF-7/ADR and MCF-7 cells, respectively. Owing to the efflux of doxorubicin by P-gp, the intracellular concentration of doxorubicin in MCF-7/ADR cells was only 0.42 $\pm$ 0.03 μg per mg protein after 24 h of incubation, which was significantly lower than that seen in MCF-7 cells after incubation with free doxorubicin for the same period (3.61 $\pm$ 0.41 μg per mg protein). A much higher intracellular accumulation of doxorubicin and its equivalent was observed in MCF-7/ADR cells after incubation with doxorubicin-tethered AuNPs, though the value was slightly lower in MCF-7 cells in the same conditions. When incubated with DOX-Hyd@AuNPs or DOX-Cbm@AuNPs, the cellular amount of doxorubicin (or equivalent) in MCF-7/ADR cells increased rapidly with the extension of culturing time, reaching 2.57 $\pm$ 0.04 and 2.83 $\pm$ 0.21 μg per mg protein, respectively, which was about 6 times higher than the value after free doxorubicin

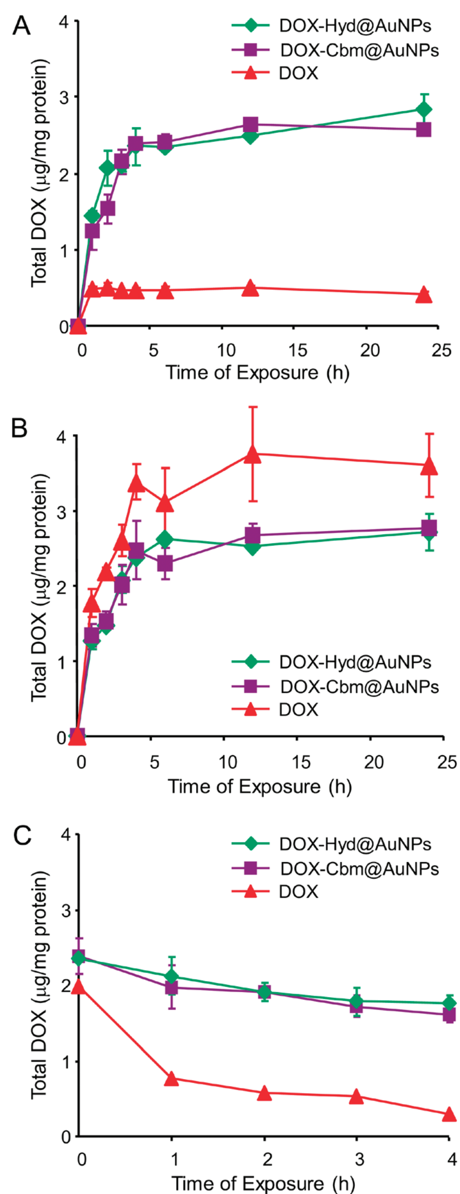

Figure 5. (A and B) Comparison of total doxorubicin (DOX) accumulation in MCF-7/ADR cells (A) and MCF-7 cells (B) after incubation with free DOX, DOX-Hyd@AuNPs, or DOX-Cbm@AuNPs for different periods of time. The concentration of DOX (free DOX or equivalent) in cell culture was 5 μg mL^{-1} in all the experiments. (C) Retention of DOX in MCF-7/ADR cells after preincubation with DOX, DOX-Hyd@AuNPs, or DOX-Cbm@AuNPs for 4 h. The concentration of total DOX (free DOX and equivalent DOX in polymeric conjugate form) in the free DOX preincubation was 40 μg mL^{-1}, while it was 5 μg mL^{-1} for DOX-tethered AuNPs. Three independent experiments were performed.

treatment. Furthermore, the cellular amounts of doxorubicin (free DOX or equivalent in polymeric conjugate form) in MCF-7/ADR cells and MCF-7 cells were very similar. These results indicated that doxorubicin-tethered AuNPs might not be the substrate of P-gp, thus they could be retained in the MDR cells after internalization.

In another experiment, we determined how doxorubicin (or equivalent) was retained in MCF-7/ADR cells with the delivery of doxorubicin-tethered AuNPs.

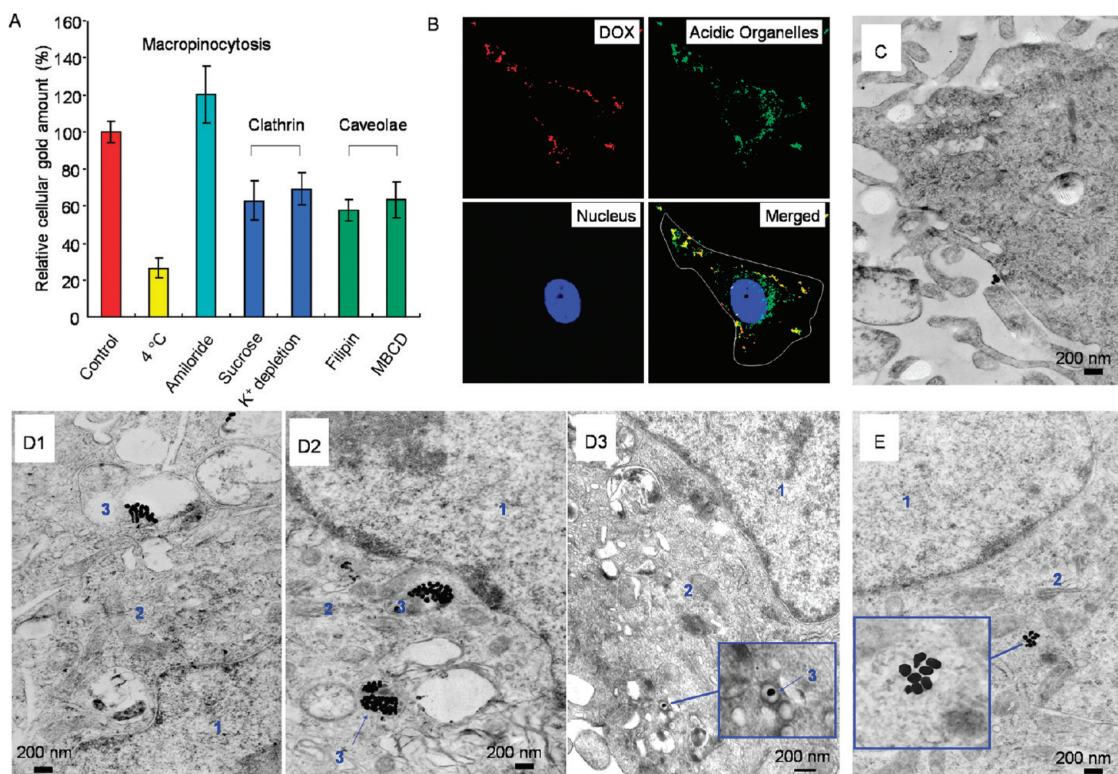

Figure 6. (A) Cellular amount of AuNPs in MCF-7/ADR cells after 4 h of incubation with DOX-Hyd@AuNPs. Cells were incubated either at 37 °C (control) or at 4 °C. Prior to the incubation with DOX-Hyd@AuNPs at 37 °C, cells were pretreated with sucrose, potassium depletion, filipin, methyl-β-cyclodextrin (MBCD), or amiloride. (B) Confocal images showing cellular uptake of nanoparticles (red) by MCF-7/ADR cells after 4 h of incubation with DOX-Hyd@AuNPs at 37 °C. The acidic organelles were stained with Lysotracker Green (green), and the cell nuclei were counterstained with 4′,6-diamidino-2-phenylindole (DAPI, blue). (C, D, E) MCF-7/ADR cells observed by transmission electron microscopy. (C) The cells were cultured with DOX-Hyd@AuNPs for 12 h. AuNPs were located in the extracellular region before endocytosis. (D1–D3) DOX-Hyd@AuNPs were located in large (>1000 nm, D1), medium (150 to 1000 nm, D2) and small (<150 nm, D3) vesicles. (E) The cells were cultured with DOX-Hyd@AuNPs for 24 h. AuNPs escaped from vesicles and localized in the cytosol. Sections 1, 2, and 3 in D1–D3 and E indicate the cell nucleus, cell cytosol, and vesicles, respectively.

MCF-7/ADR cells were incubated with either free doxorubicin or doxorubicin-tethered AuNPs for 4 h and the cells were subsequently washed with PBS to remove uninternalized free doxorubicin or doxorubicin-tethered AuNPs. The cells were further incubated in fresh cell culture medium for different periods of time (from 1 to 4 h). It is noteworthy that we maintained the initial doses of doxorubicin at 5 μg mL^{-1} in treatments with doxorubicin-tethered AuNPs but intentionally increased the initial concentration of doxorubicin to 40 μg mL^{-1} in the free doxorubicin treatment to increase the initial cellular doxorubicin level. As shown in Figure 5C, a fast decline in intracellular doxorubicin level was observed in MCF-7/ADR cells preincubated with free doxorubicin as a result of drug efflux by P-gp. Only 15.1 $\pm$ 1.6% doxorubicin was retained in the cells after 4 h of incubation in the free doxorubicin treatment. However, the amount and the efflux rate of doxorubicin were significantly lower when the cells were preincubated with doxorubicin-tethered AuNPs, where cells retained about 68.0 $\pm$ 4.5% and 75 $\pm$ 4.5% doxorubicin (free DOX or equivalent DOX in polymeric conjugate form) after 4 h of incubation, indicating the efflux of doxorubicin was decreased upon its immobilization on AuNPs. These results demonstrated that tethering doxorubicin onto the surface of AuNPs protected it against efflux by P-gp, thus the nanoparticles increased the cellular retention of doxorubicin in MCF-7/ADR cells.

Internalization and Intracellular Drug Release of Doxorubicin-Tethered AuNPs. We next demonstrated that doxorubicin could be released from DOX-Hyd@AuNPs in response to the intracellular acidic microenvironment during or after its accumulation in MCF-7/ADR cells. In considering this point, a cellular entry following acidic organelle formation is probably the prerequisite for triggered intracellular drug release *via* the breakage of hydrazone bonds. We then investigated the entry mechanism of DOX-Hyd@AuNPs into MCF-7/ADR cells. Endocytosis is known as one of the important entry mechanisms for various extracellular materials, particularly nanoparticles, which is energy dependent and can be hindered when incubation is performed at low temperatures (*e.g.*, 4 °C instead of 37 °C).[45] As shown in Figure 6A, incubation of DOX-tethered AuNPs at 4 °C for 1 h resulted in significant depressed internalization of AuNPs to 26.5 $\pm$ 5.4% of the control, which involved incubation of DOX-Hyd@AuNPs with MCF-7/ADR cells

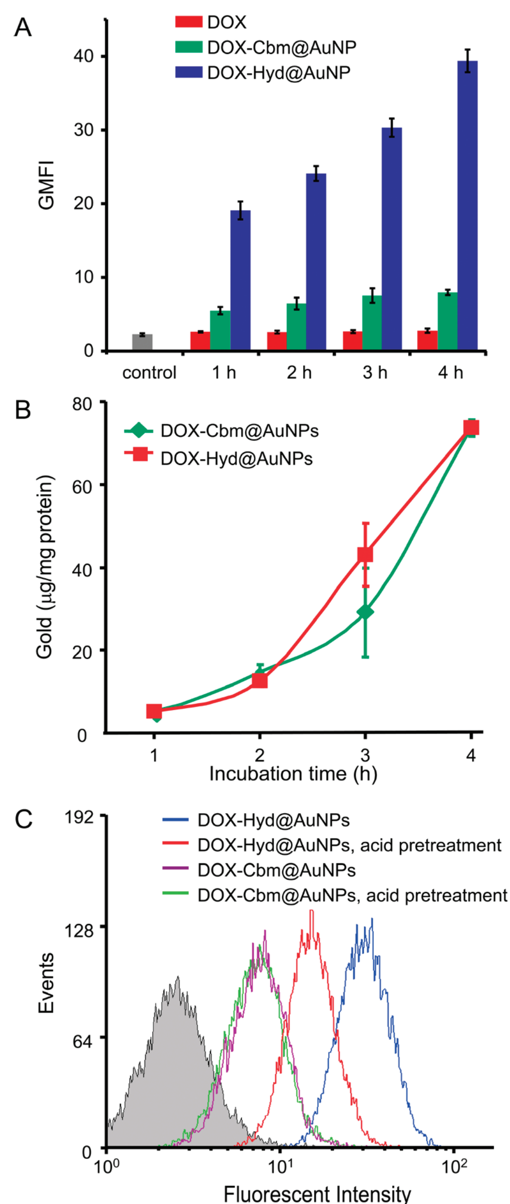

Figure 7. (A) Geometric mean fluorescence intensity (GMFI) of MCF-7/ADR cells after incubation with free doxorubicin (DOX) and doxorubicin-tethered AuNPs for various periods of time. The dose of doxorubicin or its equivalent was 5 μg mL^{-1}. Data were collected from flow cytometric analyses (n = 3). (B) Determination of cellular amount of AuNPs in MCF-7/ADR cells after incubation with doxorubicin-tethered AuNPs for various periods of time at a doxorubicin or its equivalent dose of 5 μg mL^{-1} (n = 3). (C) Flow cytometric analyses of MCF-7/ADR cells after incubation with doxorubicin-tethered AuNPs for 1 h with or without preincubation at pH 5.0. The dose of doxorubicin or its equivalent was 5 μg mL^{-1}.

at 37 °C for 1 h where cellular amounts of AuNPs were analyzed by inductively coupled plasma mass spectrometry (ICP-MS). This result suggested that DOX-Hyd@AuNPs entered the cells *via* energy-dependent endocytosis.

The endocytosis pathway encompasses several subcategories, including phagocytosis, pinocytosis, clathrin-dependent receptor-mediated and caveolae-dependent endocytosis; phagocytosis is always attributed to the endocytosis of large particles,[46] which was not tested in this work. As shown in Figure 6A, amiloride, an inhibitor of pinocytosis,[47] did not show an obvious effect on the endocytosis of DOX-Hyd@AuNPs, demonstrated by a similar cellular level of AuNPs (120.3 ± 15.35%) to the control group. However, sucrose treatment or potassium depletion of the cells, which are known to perturb clathrin-mediated endocytosis,[48] caused around a 40% decrease in the uptake of the AuNPs. Pretreatment of the cells with filipin or methyl-β-cyclodextrin (MBCD), both reported to block caveolae-mediated uptake,[49] prior to the incubation with DOX-Hyd@AuNPs also had a significant effect on their uptake by MCF-7/ADR cells, exhibiting 42.6 ± 5.65% and 36.4 ± 9.13% reductions, respectively, when compared with the control. These data indicated that both caveolae and clathrin mediated the internalization of DOX-Hyd@AuNPs into MCF-7/ADR cells. It must be mentioned that clathrin-mediation is known to lead to the formation of primary endosomes, which consequently form late endosomes and lysosomes that are acidic organelles with low pH values at 5.0–6.5.[46,50] The confocal laser scanning microscopy (CLSM) image of MCF-7/ADR cells shown in Figure 6B also shows that after 4 h of incubation, red fluorescence from doxorubicin was mainly localized in the acidic organelles labeled with Lysotracker Green (green).

The intracellular particle distribution of DOX-Hyd@AuNPs was further evaluated by transmission electron microscopy after exposing the nanoparticles to cells for 12 and 24 h. Figure 6C shows the nanoparticles located in the extracellular region before endocytosis. After 12 h of incubation, AuNPs were found in intracellular vesicles with different sizes, which were merely observed in the cytoplasm or nucleus (Figure 6D1-D3). Vesicles with a medium- (150 to 1000 nm) and large-size (>1000 nm) probably contribute to the formation of endosomes and lysosomes, which are important acidic organelles. It appears that some AuNPs were capable of escaping from membrane-bound vesicles and were distributed in the cytoplasm (Figure 6E).

To demonstrate our assumption that doxorubicin-tethered AuNPs can release the drug rapidly in response to the acidic environment in MDR cancer cells and in turn overcome drug resistance, we incubated free DOX or doxorubicin-tethered AuNPs with MCF-7/ADR cells and analyzed the cells using flow cytometry at different time intervals. As shown in Figure 7A, low mean fluorescence intensity was observed when the cells were incubated with free DOX at all tested time intervals from 1 to 4 h due to its poor cellular retention in MCF-7/ADR cells. On the contrary, a much enhanced fluorescence in MCF-7/ADR cells was observed after incubating the cells with DOX-Hyd@AuNPs. It is a remarkable fact that although the cellular accumulation of AuNPs in MCF-7/ADR cells was similar for treatments with either DOX-Hyd@AuNPs or DOX-Cbm@AuNPs for the

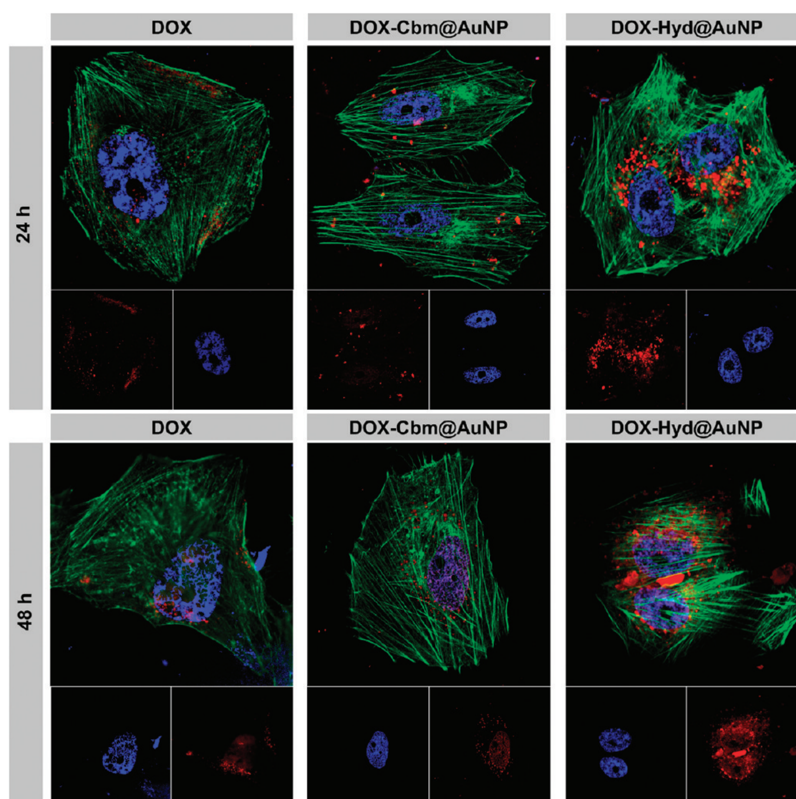

Figure 8. Confocal laser microscopic observation of MCF-7/ADR cells incubated with free doxorubicin (DOX) or DOX-tethered AuNPs for 24 and 48 h. The dose of doxorubicin or its equivalent was 5 μg mL^{-1} in the cell culture. The cells were counterstained with DAPI (blue) for the cell nucleus and Alexa Fluor 488 phalloidin (green) for the cell membrane.

same time intervals, as measured by ICP–MS (Figure 7B), the fluorescence intensity of cells treated with DOX-Cbm@AuNPs was significantly lower than that following treatment with DOX-Hyd@AuNPs at all tested time intervals. These data demonstrated that internalized DOX-Hyd@AuNPs could release doxorubicin in the acidic organelles of MCF-7/ADR cells, which would activate the fluorescence of doxorubicin quenched by AuNPs due to NSET, as illustrated in Figure 4A. However, the prevention of doxorubicin release from DOX-Cbm@AuNPs would not turn "ON" the fluorescence of doxorubicin, thus causing the lower fluorescence intensity in cells observed by FACS. The lower fluorescence intensity of cells was also observed in parental MCF-7 cells treated with DOX-Cbm@AuNPs when it was compared with the treatment of DOX-Hyd@AuNPs at all tested time intervals from 1 to 4 h. However, parental MCF-7 cells treated with free DOX at the same dose exhibited stronger fluorescence due to the nondrug resistance of MCF-7 cells (Supporting Information, Figure S10). Although the cellular reduction condition (*e.g.*, glutathione, GSH) may mediate the release of pegylated doxorubicin conjugated on the surface of AuNPs, it must be clarified that the disulfide bond linking the pegylated drug to the AuNP is much more stable than the hydrazone linkage. As shown in the Supporting Information (Figure S11), incubation of DOX-Hyd@AuNPs in PBS (pH 7.4, 0.02 M) with 20 mM GSH only led to slight increase of fluorescence intensity in 2 h incubation, likely due to the replacement of LA-PEG-Hyd-DOX from AuNPs by GSH and the subsequent recovery of fluorescence quenchment. However, much higher increase of fluorescence intensity was observed when LA-PEG-Hyd-DOX was incubated at acidic condition (pH 5.0) in the absence of GSH.

In another experiment, we mixed DOX-tethered AuNPs with the culture medium at pH 5.0 for 1 h and adjusted the pH back to pH 7.4. This medium was then submitted for culture with MCF-7/ADR cells for 1 h. We observed a significant decline in fluorescence intensity in MCF-7/ADR cells treated with the medium containing pretreated DOX-Hyd@AuNPs but not pretreated DOX-Cbm@AuNPs, when compared with cells incubated with corresponding DOX-tethered AuNPs that did not receive preincubation under acidic conditions (Figure 7C). These data provided circumstantial evidence of the responsive release of doxorubicin from DOX-Hyd@AuNPs. This is because extracellular treatment of DOX-Hyd@AuNPs at pH 5.0 led to partial extracellular release of doxorubicin but not from DOX-Cbm@AuNPs. Nevertheless, extracellular doxorubicin could not be effectively retained in MCF-7/ADR cells due to the efflux mediated by P-gp, resulting in the decline in cell fluorescence intensity in the case of cell culture pretreated with DOX-Hyd@AuNPs at pH 5.0.

In addition to the flow cytometry measurements, confocal microscopy provided visible evidence of acid

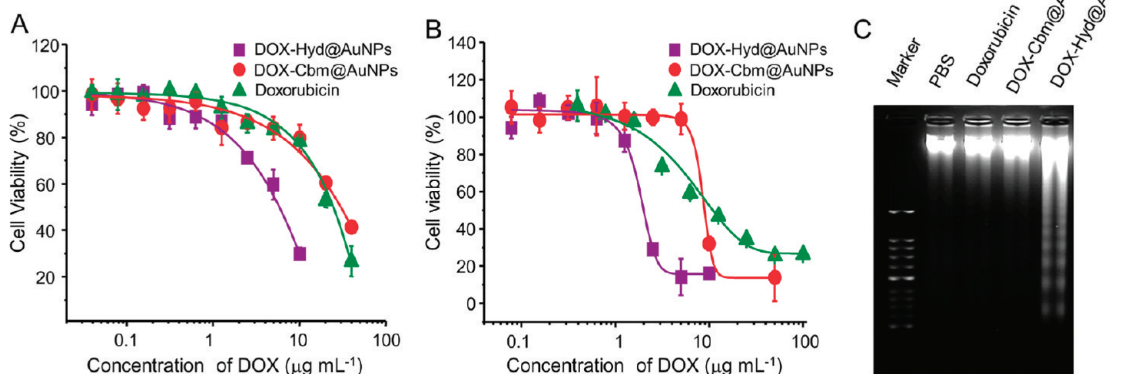

Figure 9. (A and B): Viability of MCF-7/ADR cells after treatment with free doxorubicin or doxorubicin-tethered AuNPs for (A) 48 or (B) 72 h. (C) Detection of DNA ladder formation in MCF-7/ADR cells after treatment with free doxorubicin or doxorubicin-tethered AuNPs at an equivalent concentration of 2 μg mL^{-1}.

responsive intracellular release of doxorubicin from DOX-Hyd@AuNPs. As indicated in Figure 8, MCF-7/ADR cells incubated with free doxorubicin for 24 h showed faint red fluorescence signals in the peri-membrane region, likely to be due to complex formation with P-gp, which was different to that seen in MCF-7 wild-type cells incubated with doxorubicin, where a rapid entry of doxorubicin into the cell nucleus was observed within 30 min (result not given). However, fluorescence signals were observed in the cytosol of MCF-7/ADR cells when the cells were incubated with doxorubicin-tethered AuNPs. This observation corresponds well with the above-mentioned results where doxorubicin-tethered AuNPs were shown to be internalized by and retained in MCF-7/ADR cells. Close scrutiny of the images revealed that the fluorescence signal from cells treated with DOX-Hyd@AuNPs were significantly stronger than the control groups, which were more dispersed in the peri-nuclear region. The lower fluorescence signal within the cells incubated with DOX-Cbm@AuNPs indicated that the carbamate linkage hindered the release of doxorubicin, which could not lead to an "ON" state of fluorescence due to NSET. On the contrary, doxorubicin could be released from DOX-Hyd@AuNPs in acidic organelles after being internalized and turning on the fluorescence from the quenching by the NSET. Furthermore, although fluorescence of doxorubicin could be found in the nuclei of MCF-7/ADR cells following 48 h of incubation with free doxorubicin or doxorubicin-tethered AuNPs, it was much stronger in the cell nuclei when DOX-Hyd@AuNPs was used. Considering that the interaction of doxorubicin with DNA by intercalation in the nucleus is one of the major modes of action for doxorubicin,[51,52] and that doxorubicin-tethered AuNPs might not be able to enter the nuclei, the release of doxorubicin is therefore a necessary prerequisite and is crucial in playing its role in the growth inhibition of MCF-7/ADR cells.

Enhanced Cytotoxicity and Apoptosis of MCF-7/ADR Cells Induced by DOX-Hyd@AuNPs. The above data demonstrated that the acid responsive DOX-Hyd@AuNPs enhanced drug retention in MCF-7/ADR cells and rapidly released the tethered drug into the cells. As a result, delivery of doxorubicin with DOX-Hyd@AuNPs can rapidly increase the concentration of the free drug in MCF-7/ADR cells, thereby improving its cytotoxicity and overcoming MDR in cancer cells efficiently. We incubated free doxorubicin, DOX-Hyd@AuNPs or DOX-Cbm@AuNPs at the equivalent doxorubicin doses with both MCF-7 and MCF-7/ADR cells for 48 or 72 h, and determined the half maximal inhibitory concentration of doxorubicin (IC_{50}) by MTT assay. The cytotoxicity to MCF-7 cells in response to the doses of doxorubicin is given in the Supporting Information (Figure S12). Doxorubicin showed obvious cytotoxicity to MCF-7 cells at low concentration (IC_{50} = 0.35 $\pm$ 0.16 μg mL^{-1}) after incubation for 72 h; the cytotoxicity of DOX-Hyd@AuNPs was comparable with that of doxorubicin at identical conditions (IC_{50} = 0.39 $\pm$ 0.12 μg mL^{-1}), while DOX-Cbm@AuNPs was less cytotoxic to MCF-7 cells. However, in multidrug resistant MCF-7/ADR cells, a significant decrease in the IC_{50} of DOX-Hyd@AuNPs (IC_{50} 5.12 $\pm$ 0.92 and 1.82 $\pm$ 1.68 μg mL^{-1} for 48 and 72 h, respectively) was observed when compared with free DOX treatment (IC_{50} 25.70 $\pm$ 3.42 and 10.12 $\pm$ 1.07 μg mL^{-1} for 48 and 72 h, respectively) (Figure 9 panels A and B). It must be mentioned that DOX-Cbm@AuNPs, which do not have the acid responsive doxorubicin release characteristic, did not exhibit enhanced cytotoxicity, showing an IC_{50} close to that of free doxorubicin treatment (IC_{50} 26.8 $\pm$ 2.40 and 10.85 $\pm$ 1.23 μg mL^{-1} for 48 and 72 h, respectively). It is possible that the carbamate bonds are cleaved in the cells with the aid of intracellular enzyme(s), since we could observe the intracellular release of free doxorubicin when we measured the total doxorubicin accumulation in the cells, though it was observed that most doxorubicin molecules

were still conjugated to PEG. This might explain why DOX-Cbm@AuNPs exhibited cytotoxicity but was less effective when compared with DOX-Hyd@AuNPs. On the other hand, it is also worthy of pointing out that PEG-capped AuNPs without doxorubicin conjugation did not exhibit obvious cytotoxicity to both MCF-7 and MCF-7/ADR cells after 72 h incubation (Supporting Information, Figure S13), indicating the cytotoxicity of DOX-Hyd@AuNPs would not be due to the presence of AuNPs. We also analyzed the DNA ladder formation, which is characteristic for cell apoptosis. As shown in Figure 9C, the DNA ladder formation could be detected in MCF-7/ADR cells after incubation with DOX-Hyd@AuNPs, whereas it could not be detected in cells treated with other formulations, suggesting that acid-responsive doxorubicin-tethered AuNPs could induce enhanced apoptosis of MCF-7/ADR cells.

Chemotherapeutics are crucial in combating cancer; however, drug resistance represents a major factor that limits the efficacy of chemotherapeutics. With unique properties, such as small size, high biocompatibility, low toxicity, and versatility due to the ease of surface functionalization, gold nanoparticles have been identified as promising candidates for potential clinical translation.[53,54] However, overcoming the drug resistance of cancer is still challenging. In this study, DOX-Hyd@AuNPs has been synthesized by simple chemistry. Such nanoparticles are conjugated with doxorubicin with PEG spacer, showing a small size around 30 nm. DOX-Hyd@AuNPs is insensitive to P-gp transporter-based efflux, while the retention of drug in the MDR cells is enhanced. More importantly, the acid-labile linkage between the PEG spacer and doxorubicin leads a rapid intracellular release of doxorubicin, and in turn, the delivery of doxorubicin with this system rapidly increases the intracellular drug concentration for treating drug resistant cancers. It is worth noting the PEGylation nature of this delivery system would be potentially beneficial in terms of the prolonged circulation, and it would eventually enhance its accumulation in solid tumors through the "enhanced permeation and retention" effect,[55] which needs further demonstration *in vivo*. On the other hand, this system may need further optimization to improve the bioavailability, for example, by involving active targeting of cancer-specific or overexpressed membrane proteins.

In summary, we have developed a drug delivery system by tethering doxorubicin onto the surface of AuNPs with a poly(ethylene glycol) spacer *via* an acid-labile linkage, and have demonstrated that such a delivery system can significantly inhibit the growth of multi-drug-resistant MCF-7/ADR cancer cells, owing to the high efficiency of cellular uptake by endocytosis and subsequent acid responsive release in cells. The acid response was also demonstrated using an NSET phenomenon between doxorubicin and the AuNPs. The doxorubicin-tethered AuNPs therefore served dual roles by overcoming MDR in cancer cells and probing the intracellular release of drug from the delivery system.

MATERIALS AND METHODS

Materials. α-Hydroxyl-ω-amino-poly(ethylene glycol) (HO-PEG-NH_2) and citric acid-stabilized AuNPs were prepared according to the literature.[35] *p*-Nitrophenyl chloroformate and 3-(4,5-dimethylthiazol-2-yl)-2,5-diphenyltetrazolium bromide (MTT) were obtained from Sigma-Aldrich Co. (Shanghai, China). *N*-Hydroxysulfosuccinimide (NHS) was purchased from Shanghai Medpep Co. Ltd. Hydrazine monohydrate was purchased from Sinopharm Chemical Reagent Co. Ltd. Doxorubicin hydrochloride was purchased from Zhejiang Hisun Pharmaceutical Co. Ltd. Methanol, *N,N*-dimethylformamide (DMF), and dichloromethane were dried over calcium hydride for 24 h at room temperature, followed by distillation just before use. Triethylamine (TEA) was refluxed with phthalic anhydride, then with potassium hydroxide and with calcium hydride, and distilled. Milli-Q water (18.2 MΩ) was prepared using Milli-Q Synthesis System (Millipore, Bedford, MA). α-Lipoic acid, *N,N*′-dicyclohexylcarbodiimide (DCC), and hydrogen tetrachloroaurate (III) trihydrate ($HAuCl_4 \cdot 3H_2O$) were obtained from Beijing Chemical Reagent Co., China, and used as received. All other reagents and solvents were of analytical grade and used as received.

General Characterizations. HPLC analyses of doxorubicin and the degradation of heterofunctional α-lipoyl-ω-doxorubicinyl poly(ethylene glycol) were performed with Waters HPLC system, equipped with a Waters 1525 binary pump, a Waters 2475 fluorescence detector, 1500 column heater, and a Symmetry C18 column. HPLC grade acetonitrile/water (50/50, v/v) with pH 2.7 adjusted by $HClO_4$ was used as the mobile phase at 30 °C with a flow rate of 1.0 mL min^{-1}. Fluorescence detector was set at 460 nm for excitation and 570 nm for emission and linked to Breeze software for data analysis. UV−vis absorption spectra of citric acid-stabilized AuNPs and doxorubicin-tethered AuNPs were obtained in a quartz cuvette using a Shimadzu UV 2501 spectrophotometer. TEM measurements were performed on a JEOL 2010 high-resolution transmission electron microscope with an accelerating voltage of 200 KV. The sample was prepared by pipetting a drop of the aqueous solution of nanoparticles (0.1 mg mL^{-1}) onto a 230 mesh copper grid coated with carbon and the sample was allowed to dry in air before the measurement. The fluorescence emission spectra were recorded using a Shimadzu RF-5301PC spectrofluorophotometer with an excitation wavelength at 465 nm. The amount of gold was determined using an X Series 2 ICP-MS (Thermo, Rockford, IL).

Preparation of Doxorubicin-Tethered AuNPs. LA-PEG-Hyd-DOX or LA-PEG-Cbm-DOX (1 mg) was mixed with citric acid-stabilized AuNPs (1 mg) in 10 mL of ultrapurified water at pH 8.0. The mixture was stirred in the dark for 12 h at room temperature. Thereafter, the nanoparticles were centrifuged at a speed of 14000 rpm for 15 min to remove unconjugated polymers and washed once with Milli-Q water. The concentration of unconjugated polymer was determined by HPLC analyses as described above, and the amount of conjugation at the surface of AuNPs was thus calculated.

Release of Doxorubicin from Doxorubicin-Tethered AuNPs. Doxorubicin-tethered AuNPs were incubated in phosphate buffer (0.02 M, pH 7.4) or acetate buffer (0.02 M, pH 5.0). The fluorescence emission spectra were recorded after different time intervals. To quantitatively determine the release of doxorubicin, doxorubicin-tethered AuNPs

were suspended in phosphate buffer (0.02 M, pH 7.4) or acetate buffer (0.02 M, pH 5.0) at 0.1 mg mL^{-1} in the dialysis membrane tubing (MW cutoff = 14 000, Spectrum Laboratories, Compton, CA), and the tubing was immersed in 15 mL of PBS (0.02 M, pH 7.4) or acetate buffer (0.02, pH 5.0), respectively, in a shaking water bath at 37 °C. At predetermined time points, the external buffer was collected, which was replaced with an equal volume of phosphate buffer or acetate buffer with identical pH values. The collected release medium was freeze-dried and dissolved in acetonitrile–water (50/50, v/v), and the concentration of doxorubicin was analyzed by HPLC.

Cell Culture. MCF-7 cell line was obtained from the American Type Culture Collection (ATCC, MD, USA), and the P-gp overexpressing human carcinoma cell line (doxorubicin resistant MCF-7 cell line, MCF-7/ADR) was kindly provided by Prof. Tao Zhu from the University of Science and Technology of China. The cells were cultured in RPMI 1640 medium, supplemented with 10% fetal bovine serum and 2 mM L-glutamine at 37 °C using a humidified 5% CO_2 incubator. MCF-7/ADR cells were maintained with free doxorubicin at 1 μg mL^{-1}.

Determination of the Intracellular Accumulation and Retention of Doxorubicin. MCF-7 or MCF-7/ADR cells were seeded in 24-well plates at a density of 100 000 cells/well and incubated overnight. The cells were washed with Earle's Balanced Salt Solution and treated with free doxorubicin or doxorubicin-tethered AuNPs in culture medium with equivalent doxorubicin at a concentration of 5 μg mL^{-1}. Cells were incubated at 37 °C for different periods of time, washed twice with cold PBS, and lysed in PBS containing 1% Triton X-100 at 37 °C for 30 min with three freeze–thaw cycles. The cell lysates were then treated with KCN (1 mM) for 2 h. DOX concentrations in cell lysates were measured by HPLC analyses and normalized to the total cellular protein content of the cells, which was determined by the BCA Protein Assay Kit (Pierce, Rock-ford, IL). To determine the intracellular retention of doxorubicin, MCF-7/ADR cells were cultured with either free doxorubicin or doxorubicin-tethered AuNPs for 4 h, washed with PBS, and then incubated with culture medium at 37 °C for an additional 1, 2, 3, or 4 h. Cells were lysed and the concentrations of doxorubicin in cell lysates were measured as described above.

Transmission Electron Microscopy. MCF-7/ADR cells were seeded onto 6-well plates at a density of 500 000 cells per well, after 12 or 24 h incubation with DOX-Hyd@AuNPs at a doxorubicin dose of 5 μg mL^{-1}. Excess media was removed, and the cells were washed with PBS, trypsined, and centrifuged. The cell pellets were fixed in a 0.1 M PBS solution containing 2.5% glutaraldehyde for 4 h, dehydrated through an ethanol series (70% for 15 min, 90% for 15 min, and 100% for 15 min twice) and embedded in Epon Araldite resin (polymerization at 65 °C for 15 h). Thin sections (70 nm) containing the cells were placed on the grids and stained for 1 min each with 4% uranyl acetate (1:1, acetone/water) and 0.2% Reynolds lead citrate (water), air-dried, and imaged under an 80 kV JEOL-1230 transmission electron microscope.

Flow Cytometric Analyses of Cells after Treatment with Doxorubicin or Doxorubicin-Tethered AuNPs. MCF-7/ADR cells were seeded in 24-well plates at 100 000 cells per well in 500 μL of complete RPMI 1640 medium and incubated at 37 °C in 5% CO_2 humidified atmosphere for 24 h. The media was replaced with fresh media containing free doxorubicin, doxorubicin-tethered AuNPs, or doxorubicin-tethered AuNPs after 1 h preincubation at pH 5.0 with equivalent doxorubicin at a concentration of 5 μg mL^{-1}. The cells were further incubated for specific periods of time, and then washed with PBS twice, harvested, and suspended in 200 μL of PBS for analyses using FACSCalibur flow cytometer. Cells with PBS treatment were used as control. The data were analyzed using WinMDI 2.9 software.

Analyses of Gold in Cells after Treatment with Doxorubicin-Tethered AuNPs. MCF-7/ADR cells were cultured and treated with doxorubicin-tethered AuNPs as described above. After incubation for 1, 2, 3, or 4 h, the cells were washed twice with ice-cold PBS and lysed in PBS containing 1% Triton X-100 at 37 °C for 30 min with three freeze–thaw cycles. The cellular amount of gold in cell lysates was measured by ICP–MS and normalized to the total cellular protein content of the cells, which was measured as described above.

Confocal Laser Microscopy. MCF-7/ADR cells were seeded onto 12 mm coverslips in 24-well plates with 50 000 cells per well and allowed to grow until 60% confluent. Cells were washed twice with PBS, and then incubated with free doxorubicin or doxorubicin-tethered AuNPs with equivalent doxorubicin at a concentration of 5 μg mL^{-1} in complete RPMI 1640 medium for 4, 24, or 48 h at 37 °C. Cells were washed twice with ice-cold PBS and fixed with fresh 4% paraformaldehyde for 15 min at room temperature. The cells were counterstained with 4′,6-diamidino-2-phenylindole (DAPI) for the cell nucleus, Alexa Fluor 488 phalloidin (Invitrogen, Carlsbad, CA) for the cell membrane or Lysotracker Green (Invitrogen, Carlsbad, CA) for acidic organelles following the manufacturer's instructions. The coverslips were mounted on glass microscope slides with a drop of antifade mounting media (Sigma-Aldrich Co., USA) to reduce fluorescence photobleaching. The intracellular localization was visualized under a laser scanning confocal microscope (LSM 710 Meta, Carl Zeiss Inc., Thornwood, NY).

Cell Growth Inhibition Assay. MCF-7/ADR cells were seeded in 96-well plates at 5000 cells per well in 100 μL of complete RPMI 1640 medium, and incubated at 37 °C in 5% CO_2 humidified atmosphere for 24 h. The culture medium was then replaced with 100 μL of freshly prepared culture medium containing either free doxorubicin or doxorubicin-tethered AuNPs at different doxorubicin concentrations. The cells were further incubated for 72 h, and then 25 μL of MTT (3-(4,5-dimethylthiazol-2-yl)-2,5-diphenyltetrazolium bromide, Sigma-Aldrich, Saint Louis, MO) stock solution (5 mg mL^{-1} in PBS) was added to each well to achieve a final concentration of 1 mg mL^{-1}, with the exception of the wells as blank to which 25 μL of PBS was added. After incubation for another 2 h, 100 μL of extraction buffer (20% SDS in 50% DMF, pH 4.7, prepared at 37 °C) was added to the wells and incubated for another 4 h at 37 °C. The absorbance was measured at 570 nm using a Bio-Rad 680 microplate reader. Cell viability was normalized to that of MCF-7/ADR cells cultured in complete culture media. The IC_{50} values were calculated using GraphPad Prism software (version 5.01), which were based on three separate experiments.

Cell Apoptosis Determined from DNA Fragmentation. MCF-7/ADR cells were plated in 6-well plates at a cell density of 500 000 cells per well in 2 mL of complete RPMI 1640 medium, and incubated at 37 °C in 5% CO_2 humidified atmosphere for 24 h. The culture medium was then replaced with 2 mL of freshly prepared culture media containing either free doxorubicin or doxorubicin-tethered AuNPs at a doxorubicin concentration of 2 μg mL^{-1}. After 48 h incubation, both adherent and nonadherent cells were collected, centrifuged at 5000 rpm for 5 min to pellet all the cells, and washed with PBS. Cell pellets were then resuspended in 200 μL of PBS with RNase A (0.1 mg mL^{-1}) and incubated at room temperature for 3 min. Proteinase K (1 mg mL^{-1}) and lysis buffer were added, respectively. The samples were incubated at 70 °C for 10 min, and then transferred into the DNA purification spin column (Beyotime, China) for purification, according to the manufacturer's protocol. The soluble DNA samples were subjected to electrophoresis on 1.5% agarose gel at 50 V for 2.5 h.

Acknowledgment. This work is dedicated to Professor Ren-Xi Zhuo on the occasion of his 80th birthday. This work was supported by the National Basic Research Program of China (973 Program, 2010CB934001, 2009CB930301), the National Natural Science Foundation of China (20974105, 50733003), and the Fundamental Research Funds for the Central Universities (WK2070000008).

Supporting Information Available: Syntheses procedures and characterizations of precursor polymers. This material is available free of charge *via* the Internet at http://pubs.acs.org.

REFERENCES AND NOTES

1. Cho, K. J.; Wang, X.; Nie, S. M.; Chen, Z.; Shin, D. M. Therapeutic Nanoparticles for Drug Delivery in Cancer. *Clin. Cancer Res.* **2008,** *14*, 1310–1316.
2. Peer, D.; Karp, J. M.; Hong, S.; FaroKhzad, O. C.; Margalit, R.; Langer, R. Nanocarriers as an Emerging Platform for Cancer Therapy. *Nat. Nanotechnol.* **2007,** *2*, 751–760.

3. Dong, X. W.; Mumper, R. J. Nanomedicinal Strategies to Treat Multidrug-Resistant Tumors: Current Progress. *Nanomedicine (London, U. K.)* **2010,** *5*, 597–615.
4. Fletcher, J. I.; Haber, M.; Henderson, M. J.; Norris, M. D. ABC Transporters in Cancer: More Than Just Drug Efflux Pumps. *Nat. Rev. Cancer* **2010,** *10*, 147–156.
5. Robey, R. W.; To, K. K. K.; Polgar, O.; Dohse, M.; Fetsch, P.; Dean, M.; Bates, S. E. ABCG2: A Perspective. *Adv. Drug Delivery Rev.* **2009,** *61*, 3–13.
6. Batrakova, E. V.; Kabanov, A. V. Pluronic Block Copolymers: Evolution of Drug Delivery Concept from Inert Nanocarriers to Biological Response Modifiers. *J. Controlled Release* **2008,** *130*, 98–106.
7. Batrakova, E. V.; Li, S.; Brynskikh, A. M.; Sharma, A. K.; Li, Y. L.; Boska, M.; Gong, N.; Mosley, R. L.; Alakhov, V. Y.; Gendelman, H. E.; *et al.* Effects of Pluronic and Doxorubicin on Drug Uptake, Cellular Metabolism, Apoptosis and Tumor Inhibition in Animal Models of MDR Cancers. *J. Controlled Release 143*, 290—301.
8. Kabanov, A. V.; Batrakova, E. V.; Alakhov, V. Y. Pluronic Block Copolymers for Overcoming Drug Resistance in Cancer. *Adv. Drug Delivery Rev.* **2002,** *54*, 759–779.
9. Chen, Y. C.; Bathula, S. R.; Li, J.; Huang, L. Multifunctional Nanoparticles Delivering Small Interfering RNA and Doxorubicin Overcome Drug Resistance in Cancer. *J. Biol. Chem.* **2010,** *285*, 22639–22650.
10. Meng, H. A.; Liong, M.; Xia, T. A.; Li, Z. X.; Ji, Z. X.; Zink, J. I.; Nel, A. E. Engineered Design of Mesoporous Silica Nanoparticles to Deliver Doxorubicin and P-Glycoprotein siRNA to Overcome Drug Resistance in a Cancer Cell Line. *ACS Nano* **2010,** *4*, 4539–4550.
11. Liu, Y.; Huang, L.; Liu., F. Paclitaxel Nanocrystals for Overcoming Multidrug Resistance in Cancer. *Mol. Pharmaceutics* **2010,** *7*, 863–869.
12. Li, R. B.; Wu, R. A.; Zhao, L.; Wu, M. H.; Yang, L.; Zou, H. F. P-Glycoprotein Antibody Functionalized Carbon Nanotube Overcomes the Multidrug Resistance of Human Leukemia Cells. *ACS Nano* **2010,** *4*, 1399–1408.
13. Xiong, X. B.; Ma, Z. S.; Lai, R.; Lavasanifar, A. The Therapeutic Response to Multifunctional Polymeric Nanoconjugates in the Targeted Cellular and Subcellular Delivery of Doxorubicin. *Biomaterials* **2010,** *31*, 757–768.
14. Susa, M.; Iyer, A. K.; Ryu. K.; Hornicek, F. J.; Mankin, Henry.; Amiji, M. M.; Duan, Z. F. Doxorubicin Loaded Polymeric Nanoparticulate Delivery System to Overcome Drug Resistance in Osteosarcoma. *BMC Cancer* 2009, *9*, Article No. 399.
15. Liang, X. J.; Meng, H.; Wang, Y. Z.; He, H. Y.; Meng, J.; Lu, J.; Wang, P. C.; Zhao, Y. L.; Gao, X. Y.; Sun, B. Y.;; *et al.* Metallofullerene Nanoparticles Circumvent Tumor Resistance to Cisplatin by Reactivating Endocytosis. *Proc. Nat. Acad. Sci. U.S.A* **2010,** *107*, 7449–7454.
16. Yan, Y.; Christopher, J. O.; Georgina, K. S.; Joan, K. H.; Edouard, C. N.; Frank, C. Bypassing Multidrug Resistance in Cancer Cells with Biodegradable Polymer Capsules. *Adv. Mater.* **2010,** *47*, 5398–5403.
17. Kim, D.; Gao, Z. G.; Lee, E. S.; Bae, Y. H. *In Vivo* Evaluation of Doxorubicin-Loaded Polymeric Micelles Targeting Folate Receptors and Early Endosomal pH in Drug-Resistant Ovarian Cancer. *Mol. Pharmaceutics* **2009,** *6*, 1353–1362.
18. Kim, D.; Lee, E. S.; Oh, K. T.; Gao, Z. G.; Bae, Y. H. Doxorubicin-Loaded Polymeric Micelle Overcomes Multidrug Resistance of Cancer by Double-Targeting Folate Receptor and Early Endosomal pH. *Small* **2008,** *4*, 2043–2050.
19. Sahay, G.; Alakhova, D. Y.; Kabanov, A. V. Endocytosis of Nanomedicines. *J. Controlled Release* **2010,** *145*, 182–195.
20. Zaki, N. M.; Tirelli, N. Gateways for the Intracellular Access of Nanocarriers: A Review of Receptor-Mediated Endocytosis Mechanisms and of Strategies in Receptor Targeting. *Expert Opin. Drug Delivery* **2010,** *7*, 895–913.
21. Hillaireau, H.; Couvreur, P. Nanocarriers' Entry into the Cell: Relevance to Drug Delivery. *Cell. Mol. Life Sci.* **2009,** *66*, 2873–2896.
22. Jiang, X. E.; Rocker, C.; Hafner, M.; Brandholt, S.; Dorlich, R. M.; Nienhaus, G. U. Endo- and Exocytosis of Zwitterionic Quantum Dot Nanoparticles by Live HeLa Cells. *ACS Nano* **2010,** *4*, 6787–6797.
23. Jin, H.; Heller, D. A.; Sharma, R.; Strano, M. S. Size-Dependent Cellular Uptake and Expulsion of Single-Walled Carbon Nanotubes: Single Particle Tracking and a Generic Uptake Model for Nanoparticles. *ACS Nano* **2009,** *3*, 149–158.
24. Panyam, J.; Labhasetwar, V. Dynamics of Endocytosis and Exocytosis of Poly(D,L-lactide-*co*-glycolide) Nanoparticles in Vascular Smooth Muscle Cells. *Pharm. Res.* **2003,** *20*, 212–220.
25. Yavuz, M. S.; Cheng, Y. Y.; Chen, J. Y.; Cobley, C. M.; Zhang, Q.; Rycenga, M.; Xie, J. W.; Kim, C.; Song, K. H.; Schwartz, A. G.;; *et al.*Gold Nanocages Covered by Smart Polymers for Controlled Release with Near-Infrared Light. *Nat. Mater.* **2009,** *8*, 935–939.
26. Wijaya, A.; Schaffer, S. B.; Pallares, I. G.; Hamad-Schifferli, K. Selective Release of Multiple DNA Oligonucleotides from Gold Nanorods. *ACS Nano* **2009,** *3*, 80–86.
27. Braun, G. B.; Pallaoro, A.; Wu, G. H.; Missirlis, D.; Zasadzinski, J. A.; Tirrell, M.; Reich, N. O. Laser-Activated Gene Silencing *via* Gold Nanoshell−siRNA Conjugates. *ACS Nano* **2009,** *3*, 2007–2015.
28. Kim, B.; Han, G.; Toley, B. J.; Kim, C. K.; Rotello, V. M.; Forbes, N. S. Tuning Payload Delivery in Tumour Cylindroids Using Gold Nanoparticles. *Nat. Nanotechnol.* **2010,** *5*, 465–472.
29. Aryal, S.; Grailer, J. J.; Pilla, S.; Steeberb, A. D.; Gong, S. Q. Doxorubicin Conjugated Gold Nanoparticles as Water-Soluble and pH-Responsive Anticancer Drug Nanocarriers. *J. Mat. Chem.* **2009,** *19*, 7879–7884.
30. Jain, K. K. Application of Nanobiotechnology in Cancer Therapeutics. In *Pharmaceutical Perspectives of Cancer Therapeutics*; Lu, Y., Mahato, R. I., Eds.; Springer: New York, 2009; pp 245—268.
31. Griffin, J.; Singh, A. K.; Senapati, D.; Rhodes, P.; Mitchell, K.; Robinson, B.; Yu, E.; Ray, P. C. Size- and Distance-Dependent Nanoparticle Surface-Energy Transfer (NSET) Method for Selective Sensing of Hepatitis C Virus RNA. *Chem.—Eur. J.* **2009,** *15*, 342–351.
32. Lee, H.; Lee, K.; Kim, I. K.; Park, T. G. Synthesis, Characterization, and *in Vivo* Diagnostic Applications of Hyaluronic Acid Immobilized Gold Nanoprobes. *Biomaterials* **2008,** *29*, 4709–4718.
33. Darbha, G. K.; Ray, A.; Ray, P. C. Gold Nanoparticle-Based Miniaturized Nanomaterial Surface Energy Transfer Probe for Rapid and Ultrasensitive Detection of Mercury in Soil, Water, and Fish. *ACS Nano* **2007,** *1*, 208–214.
34. Bae, Y.; Fukushima, S.; Harada, A.; Kataoka, K. Design of Environment-Sensitive Supramolecular Assemblies for Intracellular Drug Delivery: Polymeric Micelles That Are Responsive to Intracellular pH Change. *Angew. Chem., Int. Ed.* **2003,** *42*, 4640–4643.
35. Chithrani, B. D.; Ghazani, A. A.; Chan, W. C. W. Determining the Size and Shape Dependence of Gold Nanoparticle Uptake into Mammalian Cells. *Nano Lett* **2006,** *6*, 662–668.
36. Patra, C. R.; Bhattacharya, R.; Mukherjee, P. Fabrication and Functional Characterization of Gold Nanoconjugates for Potential Application in Ovarian Cancer. *J. Mater. Chem.* **2010,** *20*, 547–554.
37. Prabaharan, M.; Grailer, J. J.; Pilla, S.; Steeber, D. A.; Gong, S. Q. Gold Nanoparticles with a Monolayer of Doxorubicin-Conjugated Amphiphilic Block Copolymer for Tumor-Targeted Drug Delivery. *Biomaterials* **2009,** *30*, 6065–6075.
38. Park, C.; Youn, H.; Kim, H.; Noh, T.; Kook, Y. H.; Oh, E. T.; Park, H. J.; Kim, C. Cyclodextrin-Covered Gold Nanoparticles for Targeted Delivery of An Anticancer Drug. *J. Mater. Chem.* **2009,** *19*, 2310–2315.
39. Fan, C. H.; Wang, S.; Hong, J. W.; Bazan, G. C.; Plaxco, K. W.; Heeger, A. J. Beyond Superquenching: Hyper-Efficient Energy Transfer from Conjugated Polymers to Gold Nanoparticles. *Proc. Natl. Acad. Sci. U.S.A.* **2003,** *100*, 6297–6301.
40. Chen, Y.; O'Donoghue, M. B.; Huang, Y. F.; Kang, H. Z.; Phillips, J. A.; Chen, X. L.; Estevez, M. C.; Yang, C. Y. J.; Tan, W. H. A Surface Energy Transfer Nanoruler for Measuring Binding Site Distances on Live Cell Surfaces. *J. Am. Chem. Soc.* **2010,** *132*, 16559–16570.

41. Batist, G.; Tulpule, A.; Sinha, B. K.; Katki, A. G.; Myers, C. E.; Cowan, K. H. Overexpression of a Novel Anionic Glutathione Transferase in Multidrug-Resistant Human Breast Cancer Cells. *J. Biol. Chem.* **1986,** *261*, 5544–5549.
42. Mehta, K.; Devarajan, E.; Chen, J.; Multani, A.; Pathak, S. Multidrug-Resistant MCF-7 Cells: An Identity Crisis? *J Natl. Cancer Inst.* **2002,** *94*, 1652–1654.
43. Ke, W.; Yu, P.; Wang, J.; Wang, R.; Guo, C.; Zhou, L.; Li, C.; Li, K. MCF-7/ADR Cells (Redesignated NCI/ADR-RES) Are Not Derived from MCF-7 Breast Cancer Cells: A Loss for Breast Cancer Multidrug-Resistant Research, *Med Oncol.* DOI 10.1007/s12032-010-9747-1.
44. Gottesman, M. M.; Ling, V. The Molecular Basis of Multidrug Resistance in Cancer: The Early Years of P-glycoprotein Research. *FEBS Lett.* **2006,** *580*, 998–1009.
45. Kam, N. W. S.; Liu, Z. A.; Dai, H. J. Carbon Nanotubes as Intracellular Transporters for Proteins and DNA: An Investigation of the Uptake Mechanism and Pathway. *Angew. Chem., Int. Ed.* **2006,** *45*, 577–581.
46. Marsh, M. Clathrin-Mediated Endocytosis. In *Endocytosis*; Marsh, M., Ed.; Oxford University Press: MA, 2001; pp 1—25.
47. Walsh, M.; Tangney, M.; O'Neill, M. J.; Larkin, J. O.; Soden, D. M.; McKenna, S. L.; Darcy, R.; O'Sullivan, G. C.; O'Driscoll, C. M. Evaluation of Cellular Uptake and Gene Transfer Efficiency of Pegylated Poly-L-lysine Compacted DNA: Implications for Cancer Gene Therapy. *Mol. Pharm.* **2006,** *3*, 644–653.
48. Rejman, J.; Bragonzi, A.; Conese, M. Role of Clathrin- and Caveolae-Mediated Endocytosis in Gene Transfer Mediated by Lipo- and Polyplexes. *Mol. Ther.* **2005,** *12*, 468–474.
49. Luhmann, T.; Rimann, M.; Bitterman, A. G.; Hall, H. Cellular Uptake and Intracellular Pathways of PLL-g-PEG-DNA Nanoparticles. *Bioconjugate Chem.* **2008,** *19*, 1907–1916.
50. Brandenberger, C.; Muhlfeld, C.; Ali, Z.; Lenz, A. G.; Schmid, O.; Parak, W. J.; Gehr, P.; Rothen-Rutishauser, B. Quantitative Evaluation of Cellular Uptake and Trafficking of Plain and Polyethylene Glycol-Coated Gold Nanoparticles. *Small* **2010,** *6*, 1669–1678.
51. Ramachandran, C.; Samy, T. S. A.; Huang, X. L.; Yuan, Z. K.; Krishan, A. Doxorubicin-Induced DNA Breaks, Topoisomerase-II Activity and Gene-Expression in Human-Melanoma Cells. *Biochem. Pharmacol.* **1993,** *45*, 1367–1371.
52. Fornari, F. A.; Randolph, J. K.; Yalowich, J. C.; Ritke, M. K.; Gewirtz, D. A. Interference by Doxorubicin with DNA Unwinding in MCF-7 Breast-Tumor Cells. *Mol. Pharmacol.* **1994,** *45*, 649–656.
53. Patra, C. R.; Bhattacharya, R.; Mukhopadhyay, D.; Mukherjee, P. Fabrication of Gold Nanoparticles for Targeted Therapy in Pancreatic Cancer. *Adv. Drug Delivery Rev.* **2010,** *8*, 346–361.
54. Ghosh, P.; Han, G.; De, M; Kim, C. K.; Rotello, V. M. Gold Nanoparticles in Delivery Applications. *Adv. Drug Delivery Rev.* **2008,** *60*, 1307–1315.
55. Matsumura, Y.; Maeda, H. A New Concept for Macromolecular Therapeutics in Cancer Chemotherapy: Mechanism of Tumoritropic Accumulation of Proteins and the Antitumor Agent Amancs. *Cancer Res.* **1986,** *46*, 6387–6392.